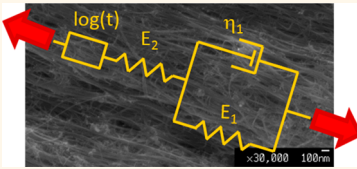


# Piezoresistive Effect in Carbon Nanotube Fibers

Agnieszka Lekawa-Raus, Krzysztof K. K. Koziol, and Alan H. Windle\*

Department of Materials Science and Metallurgy, University of Cambridge, Cambridge CB3 0FS, U.K.

**ABSTRACT** The complex structure of the macroscopic assemblies of carbon nanotubes and variable intrinsic piezoresistivity of nanotubes themselves lead to highly interesting piezoresistive performance of this new type of conductive material. Here, we present an in-depth study of the piezoresistive effect in carbon nanotube fibers, *i.e.*, yarnlike assemblies made purely of aligned carbon nanotubes, which are expected to find applications as electrical and electronic materials. The resistivity changes of carbon nanotube fibers were measured on initial loading, through the elastic/plastic transition, on cyclic loading and on stress relaxation. The various regimes of stress/strain behavior were modeled using a standard linear solid model, which was modified with an additional element in series to account for the observed creep behavior. On the basis of the experimental and modeling results, the origin of piezoresistivity is discussed. An additional effect on the resistivity was found as the fiber was held under load which led to observations of the effect of humidity and the associated water adsorption level on the resistivity. We show that the equilibrium uptake of moisture leads to the decrease in gauge factor of the fiber decrease, *i.e.*, the reduction in the sensitivity of fiber resistivity to loading.



**KEYWORDS:** carbon nanotube assemblies · carbon nanotube fibers · piezoresistivity · water effect · strain sensing

The unique physical properties of carbon nanotubes (CNTs) make them highly interesting candidates for novel nanoscale applications.<sup>1–3</sup> Even more exciting is the fact that CNTs may be assembled together and form macroscopic materials of unprecedented performance.<sup>4–7</sup> This gives the prospect for the considerable technological improvements in many areas of modern engineering. CNT fibers, *i.e.*, wirelike assemblies of axially aligned CNTs, are particularly interesting in this respect.<sup>8–10</sup> These assemblies may be used, for example, as lightweight electrical wires or for weaving of high mechanical performance conductive cloths.<sup>4,11,12</sup> However, before the CNT assemblies may be applied on a large scale their performance needs to be well explored and understood.

One of the interesting phenomena observed in CNTs is their significant piezoresistive effect (the change of resistivity upon the application of mechanical strain).<sup>13,14</sup> Depending on chirality and radius as well as deformation mode, the conductivity of nanotubes may increase/decrease or stay unchanged.<sup>15–21</sup> The attention of the researchers was particularly drawn to the fact that, in tension, some types of the CNTs show gauge factors (GF, ratio of relative change of resistivity of the material to its

deformation due to applied force) in the thousands, which is an order of magnitude larger result than for any previously known material.<sup>13,14</sup> The responses of various types of individual CNTs were well explained in terms of a distortion of their unique lattices and related changes in the bandgaps and, thus, resistivities.<sup>15–17</sup> However, this model is not easily applicable to describe the piezoresistivity of the macroscopic CNT assemblies. The difficulty of interpretation and modeling of the experimental results stems mainly from the complexity of the morphology of the assemblies. The assemblies may comprise different types of nanotubes (chirality, number of walls, length, or defects) and vary with arrangement and alignment of CNTs, densification level, or amount/type of impurities.<sup>4</sup> The overall piezoresistive effect may be influenced by all these factors.

In the following paper, we explore the piezoresistive effect in carbon nanotube fibers subject to tensile strain/stress, which until now has received little attention. The fibers were produced *via* a floating catalyst chemical vapor deposition (CVD) method and condensed *via* a liquid route (no twist applied) as described in previous works.<sup>8,22,23</sup> These fibers comprise mostly single, double-wall CNTs and some fraction of multi-wall nanotubes. The nanotubes have no

\* E-mail:  
ahw1@cam.ac.uk

Received for review July 2, 2014  
and accepted October 22, 2014.

Published online October 22, 2014  
10.1021/nn503596f

© 2014 American Chemical Society

preferential chirality and are up to 1 mm long and assembled into bundles. These hold together mainly due to van der Waals interactions as well as entanglements and friction forces. The bundles are preferentially axially aligned in the fibers (see the Supporting Information); however, there are also some entanglements and misalignments visible in the structure. The overall level of misalignment may be up to 10–20°.

Because of the high degree of longitudinal alignment of the CNTs in the fiber, it is expected that during tensile straining of the fiber most of the piezoresistive effect results from the axial strain exerted on nanotubes. According to the calculations performed of Yang *et al.*, the tensile strain should induce linear changes of the bandgap of nanotubes (thus exponential changes in resistance).<sup>15,17</sup> Armchair nanotubes are a special case for which the slope of the bandgap-strain characteristic equals 0. The slope for zigzag nanotubes is the highest and takes intermediate values for chiral nanotubes. Two thirds of zigzag and chiral nanotubes show an increase in bandgap and one-third a decrease, but some nanotubes may abruptly change the sign of slope at strains above approximately 1%. Klainer and Eggert indicated further that in the case of non-armchair but almost metallic nanotubes the change of bandgap will also be related to the radius of the nanotube.<sup>17</sup> Some of these trends predicted for individual CNTs have been confirmed experimentally by Cao *et al.*<sup>14</sup>

Most CNT assemblies comprise a selection of CNTs with randomly distributed chiralities. The overall piezoresistivity in such a case is a net effect and has to be modeled using more statistical methods. Cullinan and Culpepper<sup>24</sup> proposed that the resistance change of a sample made of many parallel single wall CNTs (SWNTs) of various chiralities which were strained simultaneously may be explained by the existence of two competing contributions. At low strains, the piezoresistive effect comes from the metallic nanotubes as they have the lowest resistance and intercept most of the current. These nanotubes first close their pseudogaps, which corresponds to resistance drop and negative GF. Next, they start to open their bandgaps and increase the resistance and GF up the point where their resistance equalizes with the semiconducting CNTs. At higher strains the closing bandgaps of semiconducting CNTs reduce back the overall resistance and the GF. These simulations predicted the maximum GF of approximately 78. The experiments, performed to test the above hypotheses and calculations, showed very similar maximum GF and an increase in resistance, however, with no sign of decrease expected for semiconducting CNTs.

The piezoresistive effect in CNT fibers is, however, even more complicated, as the CNTs never span the whole tested gauge length and they also can be

bundled, entangled, defected, impure, etc. The only tests reported up to now on fibers have been performed on the material spun from multiwall CNT arrays condensed *via* twisting (Mallik *et al.*,<sup>25</sup> Zhao *et al.*<sup>26</sup>). Both Mallik *et al.*<sup>25</sup> and Zhao *et al.*<sup>26</sup> showed an increase of resistance upon loading during basic stress–strain tests and observed maximum gauge factors of approximately 10 and 0.5, respectively.<sup>25,26</sup> Zhao *et al.* suggested that the contacts between the nanotubes play an important role as they are highly resistive and thus suppress the overall piezoresistive effect coming from carbon nanotubes.<sup>26</sup>

Here, we present an in-depth study of the piezoresistive effect in the CNT fibers. The resistance response was investigated during standard stress–strain as well as cyclic loading and relaxation experiments performed in varying atmospheric conditions. The thorough analysis of the results sheds a new light on the origin of piezoresistivity in the CNTs fibers as well as understanding the mechanical and electrical performance of the CNT fibers.

## RESULTS AND DISCUSSION

Figure 1a shows the standard stress–strain curve of a CNT fiber with corresponding resistance–strain correlation. The resistance is expressed as ratio  $R/R_0$ , which was calculated according to eq 1

$$\frac{R}{R_0} = \frac{\frac{R_0}{2} + (R_X - R_0)}{\frac{R_0}{2}} \quad (1)$$

where  $R_0$  is the initial value of resistance of the full length (40 mm) of the fiber sample before the experiment and  $R_X$  is the resistance of the full length of the sample (40 mm) measured after elongation of the fiber. Because only half of the length of the fiber was elongated in the machine (gauge length 20 mm, see the Methods),  $R_X - R_0$  represents the increase in resistance of only this elongated piece and  $R_0/2$ , its resistance right before the test. Hence, from eq 1,  $R = 2R_X - R_0$ . The same calculation method was applied throughout the rest of this paper.

During stress–strain test the resistance of the sample increases (Figure 1a). As for any conductor, the extension of the fiber renders it longer and of reduced cross section, both contributing to an increase in resistance. However, a calculation of this effect indicates that its influence is small compared with the overall resistance change recorded (Figure 1b), confirming that the observed effect is indeed a piezoresistivity (for calculations details, see the Supporting Information). Indeed, the calculation assumes constant volume, *i.e.*, a Poisson ratio of 0.5. In practice, the Poisson ratio is likely to be much less than this, so the calculation value of GF represents an upper limit.

A closer look at the resistance behavior in Figure 1a reveals that it initially lags behind strain. A similar lag is

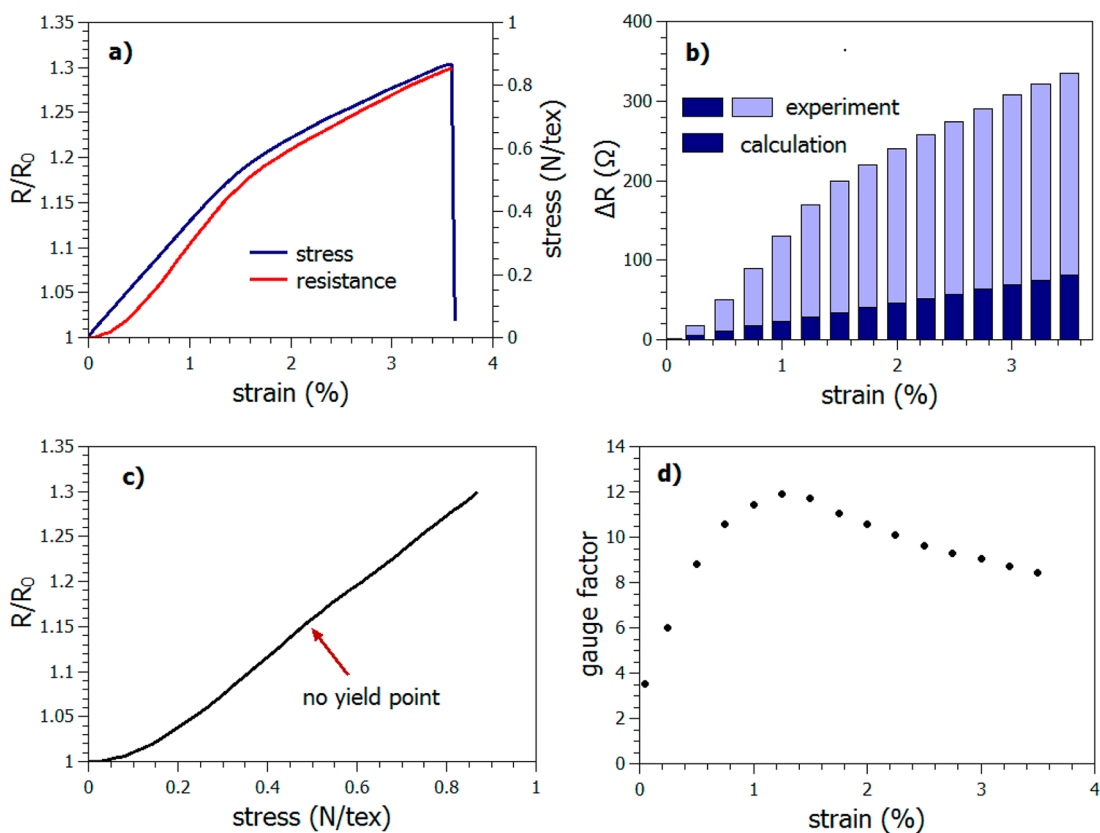


**Figure 1.** (a) Stress–strain curve and resistance change upon elongation recorded for an as-made CNT fiber sample. (b) Contribution of resistance changes due to modification of shape of the sample as a proportion of the overall measured change of resistance recorded during stress–strain testing. (c) Correlation of the corresponding resistance and stress values. (d) Change of gauge factor with strain applied to the sample.

observed when the resistance is correlated with stress as shown in Figure 1c. This curve resembles the resistance–strain/stress changes induced by opening of the bandgaps of individual CNTs reported by Yang *et al.*<sup>15,17</sup> and Cao *et al.*<sup>14</sup> If, following Cullinan and Culpepper,<sup>24</sup> we assume that most of the current is transported by metallic CNTs then the lag maybe accounted for the opening of their bandgaps. Our assumption is based on the fact that the chiralities of our CNTs are distributed randomly (statistically one-third of CNTs should be metallic). As there is no reason to expect that the stress distribution is chirality dependent we may suspect that most of the initial piezo-resistive effect comes from the metallic CNTs which by forming the least resistive pathways carry most of the current.

However, considering the morphology of our fibers, the influence of the contacts on the overall piezo-resistive effect also has to be taken into account. The recently reported research on the performance of our material in organic solvents<sup>27</sup> showed that the ingress of these liquids into the fiber causes an increase in resistance of the fibers due to first decrease in the contact area of CNT bundles and then full separation of the bundles. We may suspect that similar processes takes place due to elongation of the fiber (Figure 2).

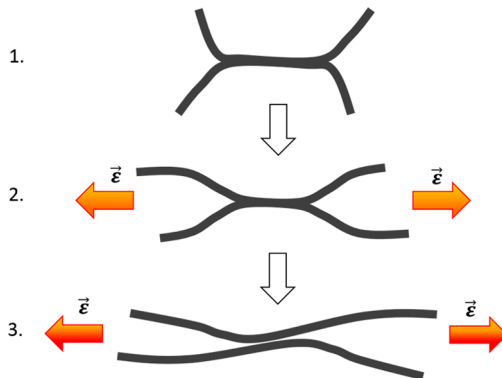


**Figure 2.** Decrease in the contact area of nonperfectly aligned CNT bundles in the fiber upon increase in strain, causing the increase in the tunneling distance for charge carriers. The effect appears to be reversible on unloading although giving rise to the hysteresis effects shown in Figure 3.

The decrease in the contact length between CNTs should cause at least a linear increase of contact resistance (according to the recent theoretical calculations of Xu *et al.*<sup>28</sup> even exponential increase). Thus, assuming a simple model of electron tunnelling between separated CNTs, we may anticipate an exponential increase in resistance with increasing distance between CNTs.<sup>29</sup> Thus, the contact phenomena should

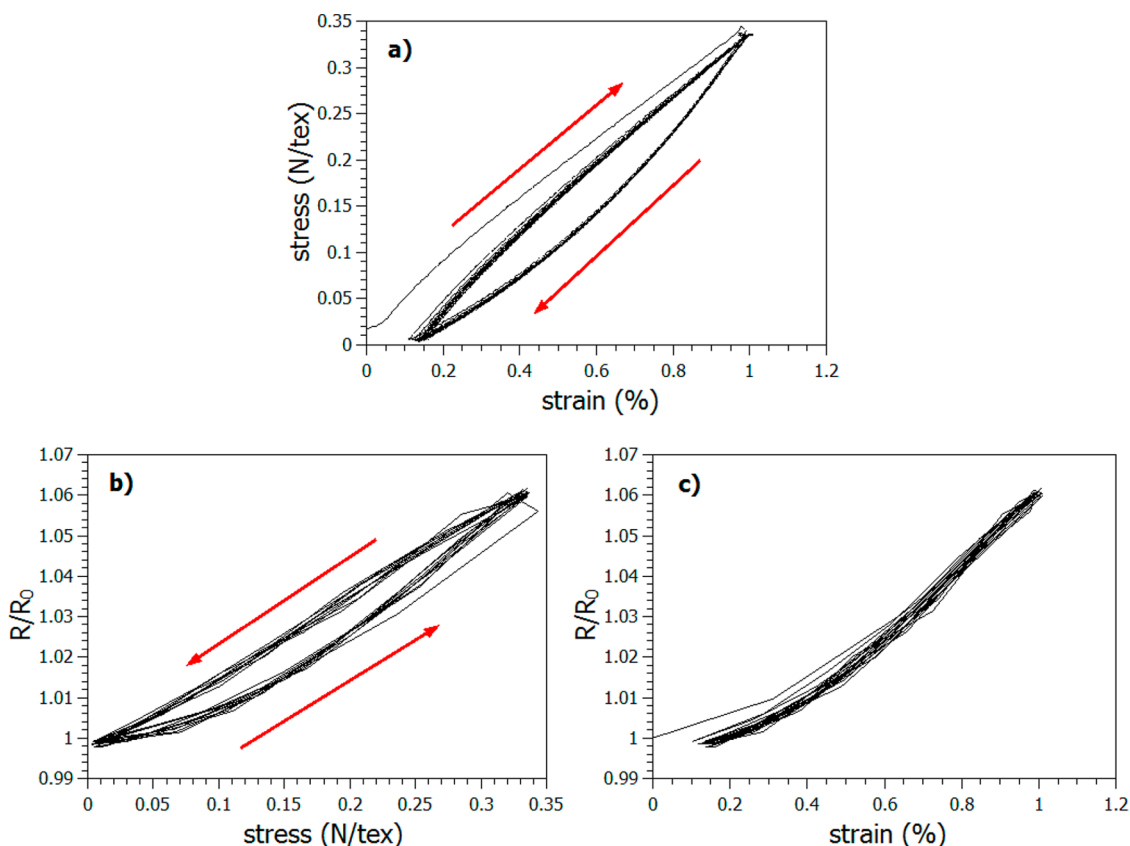


**Figure 3.** (a) Stress–strain characteristics recorded during cyclic straining test. The sample was elongated 10 times by 1% with the speed of 0.5 mm/min. (b) Correlations of relative resistance with strain. (c) Stress for the same test. The red arrows denote the loading and unloading parts of the experiment.

reinforce the resistance increase originating in metallic CNTs due to opening of their bandgaps. Taking into account the fact that the resistance of contacts will be a significant component of the overall resistance, as proposed by Zhao *et al.*,<sup>26</sup> our failure to observe the barely visible initial decrease in resistance due to closing of pseudogaps hypothesized by the Cullinan and Culpepper<sup>24</sup> may be easily accounted for. Moreover, the high contact resistance may explain why the gauge factor observed for CNT fiber (Figure 1d; for calculation details, see the Supporting Information) is much lower than the one calculated for a set of parallel, yet discrete, SWNTs.

Finally, the fact that elastic strain will reduce the contact area between bundles as envisaged in Figure 2 and therefore provide an additional component of resistance increase means that any hint of a decrease in resistance with strain (and therefore a negative GF) due to closing of the band gaps in semiconducting tubes at higher strains proposed by Cullinan and Culpepper<sup>24</sup> may well be difficult if not impossible to detect. We also have to note the possibility that the fiber breaks before both metallic and semiconducting CNTs equalize their resistances enough for the semiconducting ones to intercept the current. However, to prove this hypothesis the fibers with CNTs of controlled chiralities would have to be tested, which is currently not feasible.

The strain-induced separation of CNT bundles (or decrease in their contact area) turns out to be a very specific phenomenon. An analysis of Figure 1c shows that the plastic yielding seen in the initial stress–strain curve did not appear to imprint itself on the resistance–stress curve. This implies that the plastic strain which we relate to the realignment of CNT bundles in the fiber through sliding does not contribute to the resistivity and that the piezoresistivity is directly stress related. Two potential reasons for such behavior are the exceptional length of our CNTs and a share of misaligned and entangled CNTs. The exceptional length means that sliding, to give an overall strain of 1% would not significantly reduce the interface contact area. The share of misaligned and entangled CNTs introduce nonuniformity into the structure which produces uneven stress distribution across the fiber and may decrease the contact length in some places but also increase in others. The lack of plastic-yielding features in resistance–stress plots also indicates that the described earlier “orthogonal” pulling apart of CNT bundles which increases the tunnelling distance may be a purely elastic process.

To explore these issues further we performed several experiments. Figure 3a presents the stress–strain plot recorded during strain cycling of the sample after the initial loading curve and yield. A clear hysteresis loop

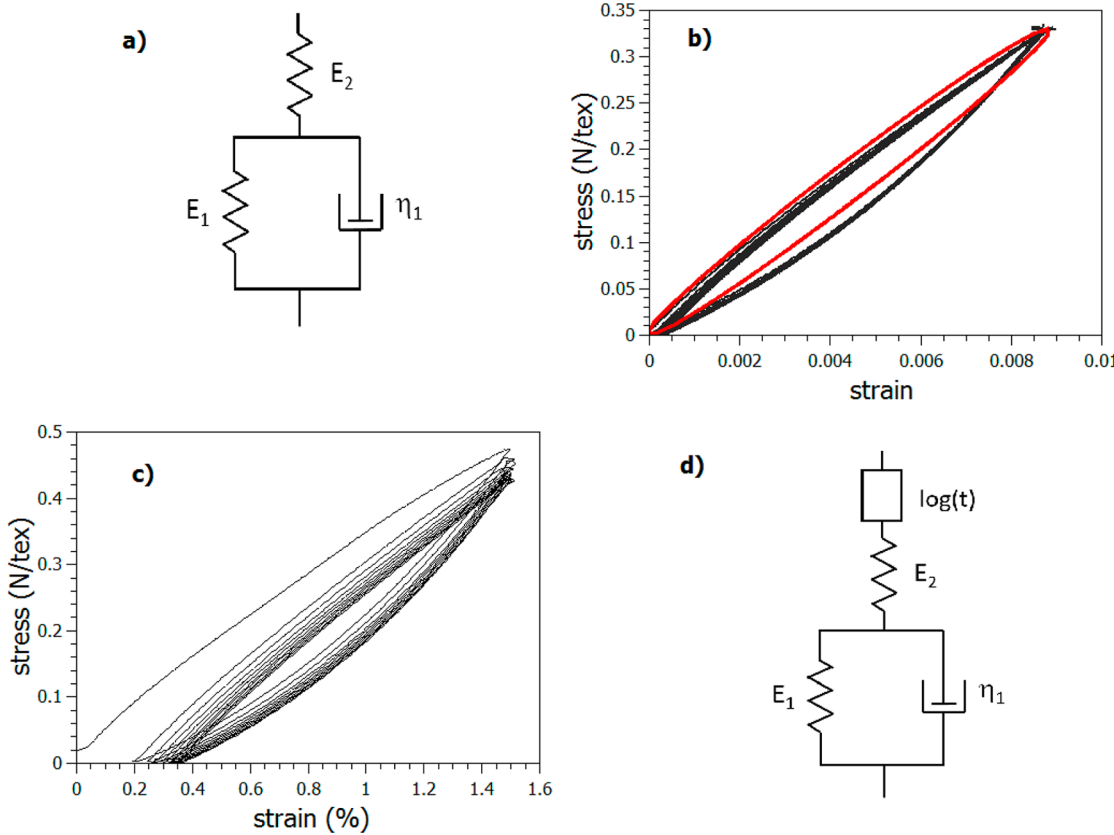


**Figure 4.** (a) Standard linear solid model used to provide fits to stress–strain plot from Figure 3a. (b) Stress–strain plot from Figure 3a (black line) and best fit obtained using the above SLS model (red line). (c) Stress–strain dependence recorded during cyclic straining of the fiber to 1.5%. (d) Extended standard linear solid model with an element simulating non-recoverable logarithmic creep.

may be observed in the plot. Interestingly, a hysteresis loop is also present in the corresponding resistance–stress plot presented in Figure 3b, where the resistance lags stress, but it is absent from resistance–strain plot shown in Figure 3c. This effect is in contrast to the behavior of the resistance on initial straining where the plastic yielding did not influence the resistance–stress plot (Figure 1c). It appears, therefore, that the resistance depends not only on stress but also on the additional strain contributing to the hysteresis loop.

In order to understand this difference more clearly, we have modeled the mechanical hysteresis behavior using a standard linear solid (SLS) model presented in Figure 4a. The constitutive equation for this model is

$$\sigma \left(1 + \frac{E_1}{E_2}\right) + \frac{\eta_1}{E_2} \dot{\sigma} = E_1 \varepsilon + \eta_1 \dot{\varepsilon} \quad (2)$$

where  $\sigma$  and  $\varepsilon$  denote stress and strain, respectively, and  $\dot{\sigma}$  and  $\dot{\varepsilon}$  their first time derivatives, while  $E_1$  and  $E_2$  stand for elastic moduli of springs and  $\eta_1$  for the viscosity characterizing the dashpot denoted in Figure 4a.

To model the dynamic behavior a sinusoidal strain/stress variation was assumed, which would be the first harmonic component of the imposed strain/stress–time plot. By finding the amplitude, period, and phase

**TABLE 1. Parameters of Basic and Extended SLS Models Which Provided the Best Fit to the Experimental Data**

test type units	model parameters				
	$E_1$ (N/tex <sup>a</sup> )	$E_2$ (N/tex)	$\tau$ (s)	$\eta_1$ (Pa·s)	$C$ (N/tex)
cyclic loading	125	44	5.4	$914 \times 10^9$	—
relaxation	202.5	37.9	6.2	$1488.4 \times 10^9$	—1

<sup>a</sup> N/tex unit is numerically equivalent to GPa.

shift, the expressions for stress and strain were established. Figure 4b shows the quality of the best fit achieved using the sinusoidal stress/strain expressions. The model parameters for the best fit listed in Table 1 were found by, first, comparison of complex moduli  $E^*$  calculated by division of the sinusoidal stress  $\sigma^*$  and strain  $\varepsilon^*$  and derived from eq 2 such as

$$\frac{\sigma^*}{\varepsilon^*} = E^* = \frac{E_1 E_2 + \tau^2 \omega^2 E_2 (E_1 + E_2)}{(E_1 + E_2) + \tau^2 \omega^2 (E_1 + E_2)} + i \frac{\tau \omega E_2^2}{(E_1 + E_2) + \tau^2 \omega^2 (E_1 + E_2)} \quad (3)$$

where  $\tau$  represents a time constant calculated as  $\eta_1/(E_1 + E_2)$ ,  $i$  is the imaginary unit, and  $\omega$  stands for the angular frequency equaling  $2\pi/T$  where  $T$  is period

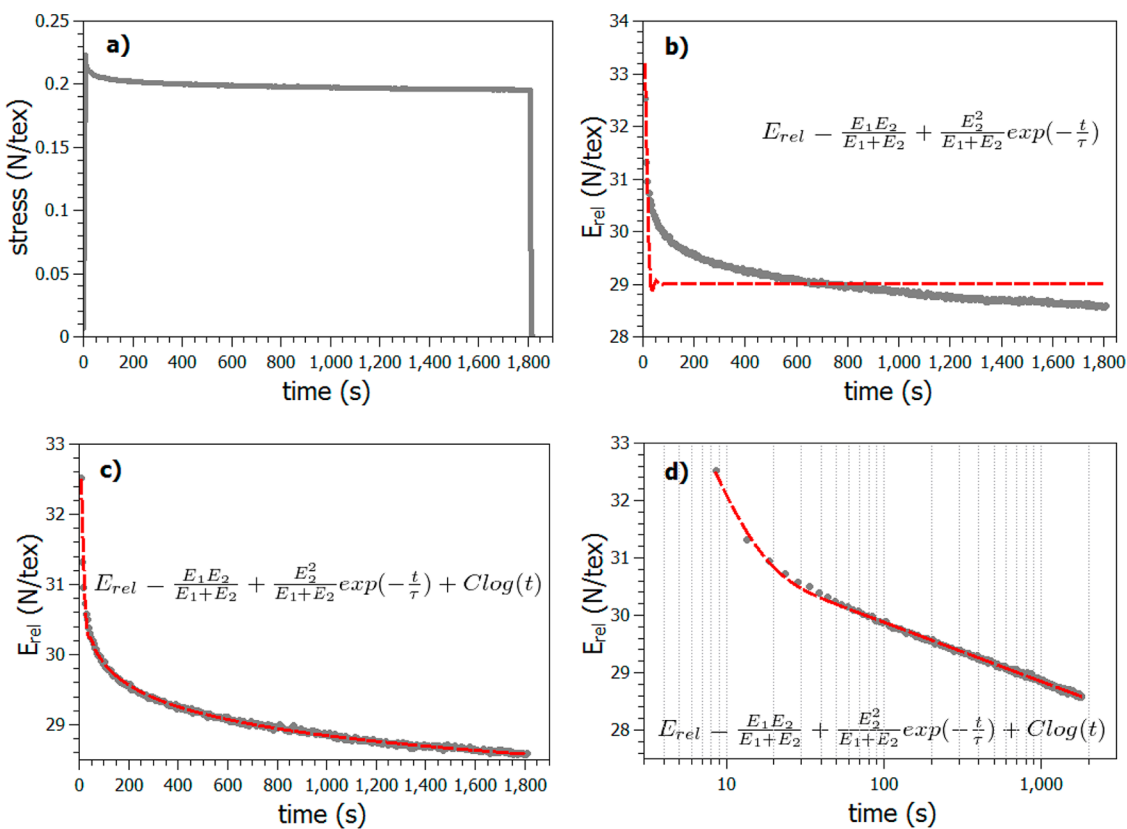


**Figure 5.** (a) Relaxation of stress in the CNT fiber sample kept under strain of 0.7% for 30 min. (b) Relaxation part of the curve in modulus units (gray line) with the best fit obtained using basic SLS model (dashed red line). (c) Relaxation curve (gray lines) on linear and (d) logarithmic time scale fitted using extended SLS model (dashed red lines).

of sinusoidal waveform (for calculations details, see the Supporting Information).

Further, assuming that the  $E_2$  spring would be the first to get extended upon elongation in the considered SLS model, the value of  $E_2$  was read from the initial loading characteristic, and the values of  $E_1$ ,  $\tau$ , and  $\eta_1$  were calculated subsequently. Because of their structure, the CNTs may definitely be considered as purely elastic components in the model so would correspond to the springs  $E_1$  and  $E_2$ . Based on the previous analysis, we may expect that the spring components will be also partly related to the strain-induced reduction in interbundle contacts. However, we also propose that this effect is responsible for the additional strain which occurs with time during a load/unload cycle and contributes to an additional increment of resistivity. We thus hypothesize that this strain component, associated with the breaking and remaking of interbundle bonds, as envisaged in Figure 2, is a nonconservative process in that energy is lost during the cycle. It is likely, given the lack of perfect order within the fiber, that there will be a wide spectrum of relaxation times, although only one is envisaged in the dashspot and spring model of Figure 4a.

A closer look at the stress-strain plot presented in Figure 3a reveals that there is a slight drift of the loops to higher strains on repeated cycles. This small

effect led us to repeat the experiment at a higher stress range, where the phenomenon was expected to be intensified (Figure 4c). The high creep observed at higher stress range (Figure 4c) confirms the expectation and would suggest that the SLS model is not fully adequate, as apart from a fully recoverable stress-strain relationships we observe some nonrecoverable contribution. We have thus explored the applicability of an extended SLS model which comprises an additional element-simulating creep (Figure 4d) and increased our time range of observation with a series of stress relaxation measurements.

Figure 5a shows the stress relaxation data for the fiber. Figure 5b shows the relaxation part of the curve represented as modulus (stress was divided by constant strain  $\varepsilon_0$  applied to the fiber), which allowed the simple fitting of the data using the equation for relaxation modulus  $E_{rel}$  derived from eq 2 which takes the form of

$$\frac{\sigma}{\varepsilon_0} = E_{rel} = \frac{E_1 E_2}{E_1 + E_2} + \frac{E_2^2}{E_1 + E_2} e^{-t/\tau} \quad (4)$$

where  $t$  represents time (for calculations details, see the Supporting Information).

Attempts to model the relaxation curve using only the SLS model, as used for cyclic loading tests, were only successful at very short times (Figure 5b).

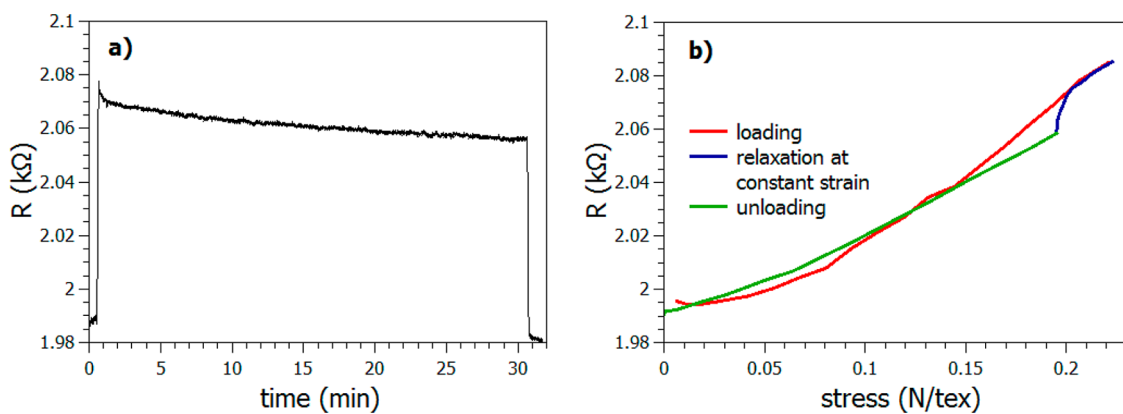


Figure 6. (a) Resistance changes during relaxation experiment presented in Figure 5. (b) Correlation of resistance and stress during loading, relaxation at constant strain, and unloading.

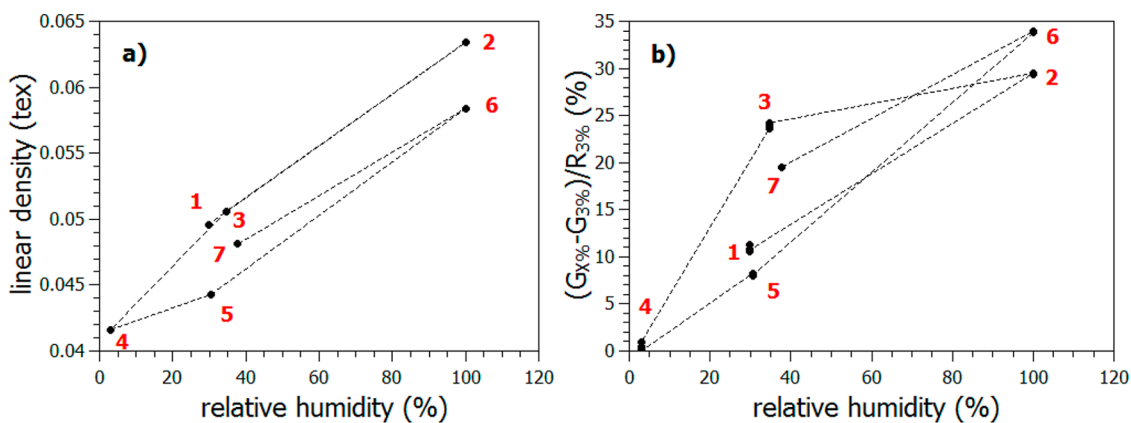


Figure 7. (a) Changes in linear density of the CNT fiber sample recorded in varying humidity conditions. The red numbers indicate the sequence of the results. (b) The corresponding RH dependent change in the resistance of the fiber. Here,  $G_{x\%}$  is the baseline conductance of the full length of the sample at given RH and  $G_{3\%}$  is the minimum conductance recorded at 3% humidity for the full length of the sample. The red numbers indicate the sequence of the results.

Here, even more clearly than in the case of dynamic tests, it appears that on top of the behavior predicted for the SLS model there is an additional creep component which continues to produce stress relaxation out to longer times. The fact that the longer time component of the behavior showed linear stress relaxation on the logarithmic plot led us to view this longer time component as a logarithmic creep behavior. The addition of such an element to the SLS as in Figure 4d allowed modeling of the overall stress relaxation. The new expression for relaxation modulus is presented in eq 5

$$E_{\text{rel}} = \frac{E_1 E_2}{E_1 + E_2} + \frac{E_2^2}{E_1 + E_2} e^{-t/\tau} + C \log(t) \quad (5)$$

where  $C$  is the scaling parameter. The best fit obtained with this model is shown in Figure 5c for linear and in Figure 5d for logarithmic scales, respectively. The values of model parameters obtained for this fit are presented in Table 1. The spring and time constants for relaxation and cyclic loading fits are very similar, which confirms that the chosen model satisfactorily describes the character of the stress/strain response of CNT fiber.

Figure 6a shows the change in resistivity during stress relaxation. It is not surprising that the resistance decreases, as the stress reduces, but at medium to longer times this decrease is considerably more than pro rata with the stress. The problems of exact replication of the magnitude of this effect from day to day led us to suspect that changes in the laboratory ambient conditions influence the experiment. By careful monitoring of the laboratory conditions and the changes of experimental results we found that relative humidity (RH) is a factor in the observations. To examine the influence of water vapor on the fiber we performed several tests under conditions of different relative humidities RH.

It was found that the fiber would take up water from the vapor. Figure 7a shows the increase in mass of the fiber for three different relative humidity ranges (0–10%, 30–40%, and 90–100%). The scatter observed in the data results mostly from the difficulty in reaching the adsorption equilibrium at given humidity. However, the presence of hysteresis in the curve cannot be entirely excluded. To confirm its presence the sorption isotherms would have to be determined.

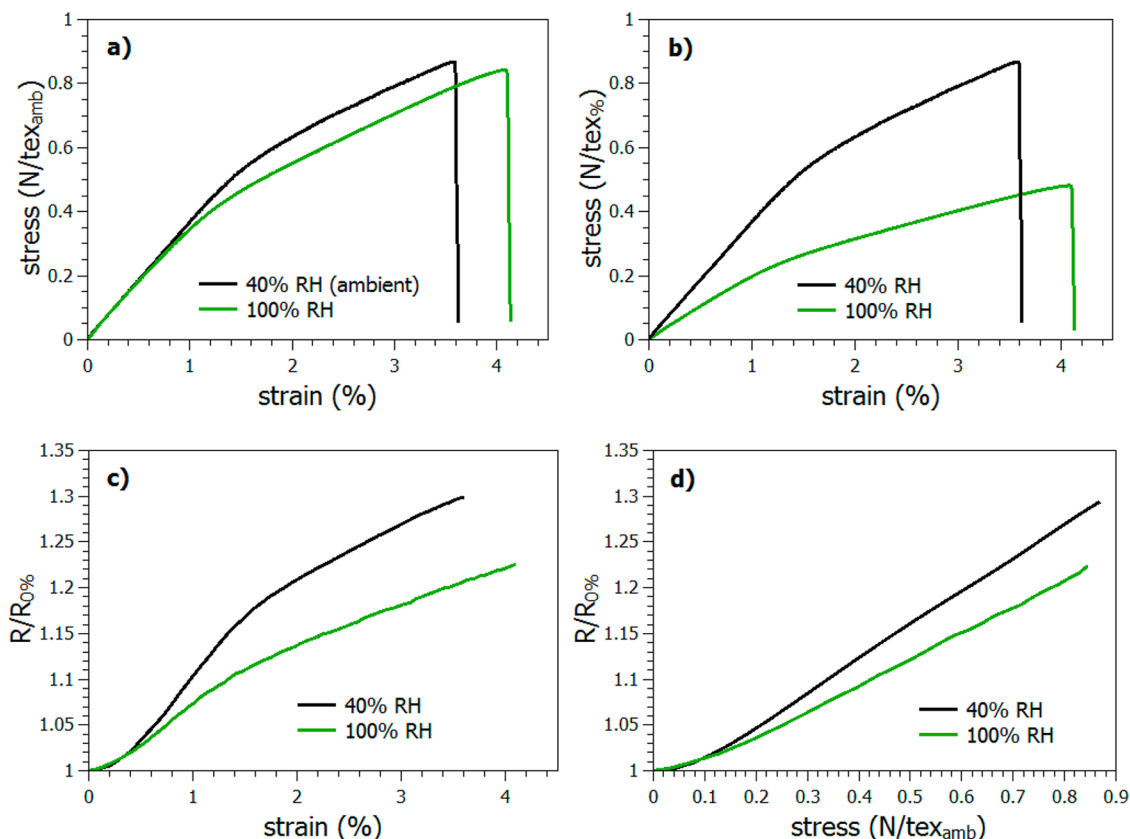


**Figure 8.** Results of the piezoresistivity tests for two similar samples of 0.04 tex measured at ambient humidity of 40%. The first sample was tested at ambient conditions and the second one at 100% RH. (a) Stress–strain curves, where stress is calculated using initial tex of the samples (recorded at ambient humidity) and (b) where stress is normalized by actual linear densities of 0.04 tex and 0.07 tex for the piece tested at 40% and 100% RH, respectively. (c) Relative resistance change correlated with applied strain and (d) stress.  $R_0\%$  is the resistance of the sample just before application of strain, *i.e.*, measured at RH in which the sample was tested.

It is remarkable that the fiber mass, as measured by the natural vibrational frequency (see the Methods), increases by some 50% when comparing saturated with dry conditions. Such high adsorption may not be entirely unexpected as the fiber is a highly porous structure with a specific surface area of 200–400  $\text{m}^2/\text{g}$ <sup>30,31</sup> mainly consisting of highly elongated, and interconnected, pores within the network of bundles. The only puzzling fact is that liquid water does not wet the fibers having contact angles slightly greater than 90°, nor does it wick as is typical of organic liquids.<sup>27</sup> However, it is widely described in the literature that water in the vapor phase (molecular state) easily adsorbs to various surfaces independent of their wettability.<sup>32</sup> While we do not examine this issue further here, we suggest that CNT fiber may adsorb water molecules like other carbon materials *via* the clustering mechanism, simultaneously, not excluding the possibility of enhancement of adsorption by the capillary condensation considering the ubiquitous existence of elongated nano- and mesoscale pores in the fiber structure.<sup>33</sup>

The presence of increasing amounts of water in the pores confirmed by the linear density measurements (Figure 7a) leads to a marked increase in electrical

conductance as shown in Figure 7b. The increase is approximately 30% with reference to the dry fiber, which indicates that conductance improvement is approximately proportional to the increase in sample weight. These results are in contrast to the mechanical performance of the fiber upon water uptake. Figure 8a shows stress–strain curves of two similar samples tested at ambient RH (40%) and at 100% RH. The difference in the curves is very small if the stress is presented as force per linear density of these samples recorded at ambient RH (*i.e.*, 0.04 tex). If, however, the stress of the second sample is calculated on the basis of its linear density after the water content is increased in the 100% RH (0.07 tex), the specific stress levels are reduced, as the fiber contains mechanically redundant water, which adds to weight but not strength (Figure 8b). The differing influence of water adsorption on electrical and mechanical properties produce changes in the piezoresistive effect of the fiber. Parts c and d of Figure 8 show the resistance–strain and resistance–stress correlations for the above analyzed samples. While the characteristic features of these curves such as initial exponential increase of resistance and further hints of plastic yielding in the resistance strain curves are similar, the increase in

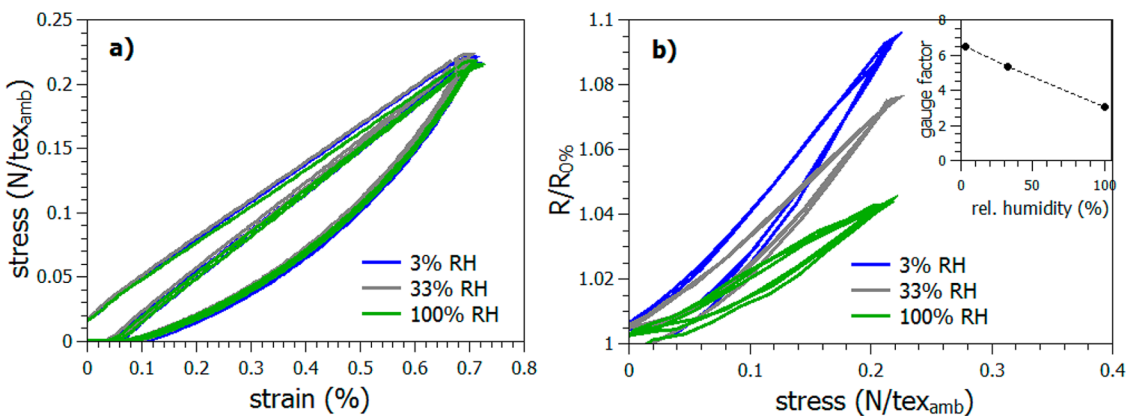


Figure 9. (a) Three examples of stress–strain hystereses recorded for the same sample at ambient humidity (0.052 tex) in 3% RH after current annealing (0.047 tex) and at 100% RH (0.067 tex). Stress for all curves is normalized by tex recorded at ambient humidity before the experiment. (b) Correlations of changes in relative resistance and normalized stress. Resistance  $R_{0\%}$  is the resistance of the sample just before application of strain measured at RH in which the sample was tested.

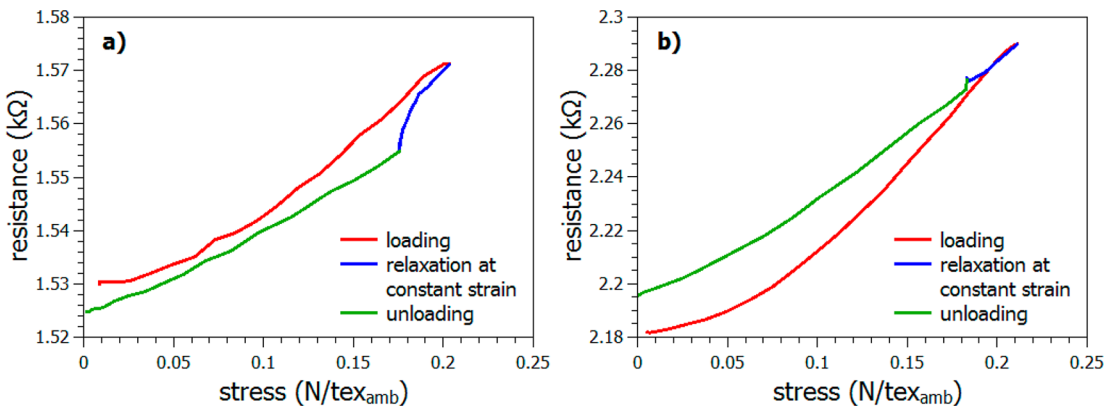


Figure 10. Relaxation test performed on the fiber (presented before in Figure 5/6) (a) at 100% RH (0.079 tex) and (b) in fully desorbed state (0.029 tex). The graphs show correlations of resistance and stress normalized by tex of 0.054 recorded at ambient humidity before the experiment.

resistance relative to the resistance recorded at the given humidity is significantly lower at 100% compared with 40% RH. This implies that not only the absolute value of resistance decreases with increasing water uptake but also that the water does not play a direct role in the piezoresistivity.

Analogous observations are true for cyclic loading tests performed on the fibers at varying humidity of 3%, 33%, and 100%. There are no discernible differences in stress–strain plots (Figure 9a) including no changes in the width of hystereses loops. However, the correlations of resistance and stress (Figure 9b) show a clear decrease with increasing humidity in the sensitivity of resistance to applied stress, with no change in the characteristic shape of these plots and width of hystereses loops. The suppressed piezoresistivity will be also reflected in the gauge factor. The dependence of gauge factors on RH calculated for maximum elongations at each humidity is presented in the inset.

Finally, the relaxation tests were performed at the same piece of fiber (as presented in Figures 5 and 6) at 100% and 3% RH (Figure 10). The absence of an increased reduction in resistance during relaxation about

that pro rata with stress, in the dry 3% fiber, was not an intrinsic property of a CNT fiber. We suggest that the fiber is able to adsorb additional water when held under stress.

The results of the above experiments imply that ambient humidity interferes with the piezoresistive effect as the water adsorbates decrease the resistivity of the fiber while not influencing stress and strain. Moreover, the sensitivity of the fiber resistivity to load decreases proportionally to the amount of adsorbed water. Nevertheless, the conclusions regarding the nature of piezoresistivity in the CNT fiber drawn at the beginning are not changed. First, the characteristic dependencies of resistance on stress and strain are not qualitatively different from the ones observed at ambient humidity. This indicates that the conclusion regarding the important role of CNTs and their changing contact area as well as nonuniform stress distribution across the fiber would still hold. The fact that in very dry conditions the GF increases is also not changing the applicability of hypothesis pointing at the role of high contact resistance between CNT bundles. The increase of GF from ambient down to 3% humidity was

approximately 30%. The maximum GF we observed at our ambient humidity tests amounted to 15. This number increased by 30% gives not more than 20 GF, which is still much lower than the value predicted by Cullinan and Culpepper<sup>24</sup> for a parallel set of strained SWNTs indicating that the network structure of our fibers plays an important role. This conclusion raises, however, a basic physics question about the mechanism responsible for the improvement of conductivity of CNT fiber upon water adsorption,<sup>34</sup> which will be the topic of a future paper.

## CONCLUSIONS

The resistivity of carbon nanotube fibers, spun directly from the floating catalyst CVD zone, has been measured as a function of the applied axial strain/stress. As expected from the theoretical and experimental literature, the overall resistance rises with increasing strain/stress. Initially, the resistance–strain/stress curves show an exponential growth consistent with the opening of bandgaps of metallic CNTs and decrease in the contact area of CNT bundles. Further, the resistance increases proportionally to strain/stress showing clear change in slope at the point at which fiber plastically yield in the resistance–strain plot. The overall shape of the resistance–strain curve and gauge factor–strain dependence may suggest that the effect of changing contact area of CNT bundles overwhelms the resistance decrease resulting from the straining of semiconducting CNTs. However, the prevailing contribution of metallic CNTs may not be fully disregarded at this stage. The fact that the overall gauge factor is low may be accounted for the high-contact resistance between the nanotubes as suggested before. Finally, in the case of resistance–stress dependence the resistivity was not found affected by the plastic yielding of the fiber on first loading. The observation that the sliding of CNTs related to plastic deformation does not have an influence on resistance is understood in the terms that for very long CNTs (length/diameter  $>10^5$ ) the sliding associated with  $\sim 1\%$  axial strain will not significantly influence the contact area.

However, the strain component of the hysteresis loop on cyclic loading, typical of this type of fiber, does

lead to an added component of resistivity. We correlate this behavior with the change in the “orthogonal” contact area between CNT bundles upon loading, a process, which although reversible, is likely to be associated with a time constant as bonds have to be remade on recovery. The fiber also shows a degree of creep, which was best observed as stress relaxation under load. However, the creep strain observed in this way led to a reduction in resistivity exactly as would be expected from simply reduction in stress, at least over short times.

The mechanical performance of the fiber was modeled using a standard linear solid to which an extra element had been added in series to account for the creep behavior of the fiber, which would appear to be logarithmic with time.

The “short times” caveat in relaxation tests is necessary as at longer times under laboratory conditions, the decrease in resistivity, during stress relaxation, began to outstrip the decrease in stress. It was noted that this effect was dependent on the laboratory humidity, which led to a series of tests at different humidities. With a contact angle slightly greater than 90° water neither wicks nor wets the fiber, yet it very clearly enters the fiber in the vapor phase leading to very significant tex variations. As long as at higher humidities up to 100%, the additional reduction in resistivities at longer times under load was associated with the uptake of water during the tests at the lowest achievable humidity of 3%, the change in resistivity followed the reduction in stress quite closely. Further analysis showed that the uptake of water decreases the overall sensitivity of fiber resistance to loading. We conclude, however, that while humidity influenced the conductivity of the fiber during resistance–strain tests it is only an additional phenomenon to the true piezo-resistive effect taking place in the fibers. The piezo-resistivity observed in CNT fibers is very much affected by the specific morphology of this material and therefore is potentially induced both by the straining of its individual constituents, CNTs, which are the load carriers in the fiber, and strain-induced change in the contact area between CNT bundles.

## METHODS

The mechanical measurements on the fiber were performed using a Textechno FAVIMAT, an instrument used in the textile industry for measurements of linear density and tensile testing of fibers.<sup>35</sup> The resolution of load measurements was 0.0001 cN, and the elongation was recorded with an accuracy of 0.1  $\mu\text{m}$ . The machine applied a vibration method to measure linear density of the fibers. The operation of the FAVIMAT was remotely controlled with a software package provided by the supplier. For all tests, the gauge length was set to 20 mm. However, the overall length of the fiber samples between electrical contacts was 40 mm to ensure that only the fiber, and not the contacts, was subjected to mechanical forces applied by the FAVIMAT.

Before the tests the samples were connected with the aid of silver paint to very thin copper wires, which were attached with adhesive tapes to the machine to avoid any undesirable tension on the fiber. Further, the fiber–copper sample was attached to an electrical test circuit and clamped in the grips of Favimat. The results of both the electrical and mechanical measurements were logged in a computer for further processing.

For the testing of the fiber in very low and high humidity the front niche of the machine was covered with a Plexiglas window. Thus, a sample under test was enclosed in a partly sealed chamber. A dry atmosphere was obtained in the chamber by the constant pumping of artificial air of less than 3% relative humidity (RH). The fibers were additionally annealed with DC current of about 10 mA for 20–30 min. To achieve

maximum humidity, containers with deionized water and cloths soaked with water were placed in the chamber. Additionally, water-enriched atmospheric air was constantly pumped into the chamber. The fiber was tested when condensation of water vapor was visible on the front window. The relative humidity was additionally monitored by an electronic RH meter placed in the chamber under the FAVIMAT grips. Testing in atmospheric humidity of 30–40% was performed without the Plexiglas window. All of the measurements were carried out when the resistance of the fiber was approximately stabilized at a given RH, which could take from several hours to 3 days.

*Conflict of Interest:* The authors declare no competing financial interest.

*Supporting Information Available:* Details of calculations. This material is available free of charge via the Internet at <http://pubs.acs.org>.

*Acknowledgment.* A.L.-R. acknowledges Trinity College, University of Cambridge, for a Coutts Trotter Studentship. A.L.-R. and K.K.K.K. thank and European Research Council (under the Seventh Framework Program FP7/2007–2013, ERC grant agreement no. 259061) for funding. K.K.K.K. thanks the Royal Society for further financial support.

## REFERENCES AND NOTES

- Wang, H.; Wei, P.; Li, Y.; Han, J.; Lee, H. R.; Naab, B. D.; Liu, N.; Wang, C.; Adjianto, E.; Tee, B.; et al. Tuning the Threshold Voltage of Carbon Nanotube Transistors by n-Type Molecular Doping for Robust and Flexible Complementary Circuits. *Proc. Natl. Acad. Sci. U.S.A.* **2014**, *111*, 4776–4781.
- Kreupl, F. Electronics: The Carbon-Nanotube Computer has Arrived. *Nature* **2013**, *501*, 495–496.
- Kong, J.; Franklin, N. R.; Zhou, C.; Chapline, M. G.; Peng, S.; Cho, K.; Dail, H. Nanotube Molecular Wires as Chemical Sensors. *Science* **2000**, *287*, 622–625.
- Lekawa-Raus, A.; Patmore, J.; Kurzepa, L.; Bulmer, J.; Koziol, K. Electrical Properties of Carbon Nanotube Based Fibers and Their Future Use in Electrical Wiring. *Adv. Funct. Mater.* **2014**, *24*, 3661–3682.
- Lu, W.; Zu, M.; Byun, J.-H.; Kim, B.-S.; Chou, T.-W. State of the Art of Carbon Nanotube Fibers: Opportunities and Challenges. *Adv. Mater.* **2012**, *24*, 1805–1833.
- Janas, D.; Koziol, K. A Review of Production Methods of Carbon Nanotube and Graphene Thin Films for Electro-thermal Applications. *Nanoscale* **2014**, *6*, 3037–3045.
- Lan, Y.; Wang, Y.; Ren, Z. F. Physics and Applications of Aligned Carbon Nanotubes. *Adv. Phys.* **2011**, *60*, 553–678.
- Li, Y.-L.; Kinloch, I. A.; Windle, A. H. Direct Spinning of Carbon Nanotube Fibers From Chemical Vapor Deposition Synthesis. *Science* **2004**, *304*, 276.
- Zhang, M.; Atkinson, K. R.; Baughman, R. H. Multifunctional Carbon Nanotube Yarns by Downsizing an Ancient Technology. *Science* **2004**, *306*, 1358.
- Ericson, L. M.; Fan, H.; Peng, H.; Davis, V. A.; Zhou, W.; Sulpizio, J.; Wang, Y.; Booker, R.; Vavro, J.; Guthy, C.; et al. Macroscopic, Neat, Single-Walled Carbon Nanotube Fibers. *Science* **2004**, *305*, 1447.
- Dalton, A. B.; Collins, S.; Muñoz, E.; Razal, J.; Ebron, V. H.; Ferraris, J.; Coleman, J.; Kim, B. G.; Baughman, R. Super-Tough Carbon-Nanotube Fibres. *Nature* **2003**, *423*, 703.
- Mylvaganam, K.; Zhang, L. C. Ballistic Resistance Capacity of Carbon Nanotubes. *Nanotechnology* **2007**, *18*, 475701.
- Obitayo, W.; Liu, T. A Review: Carbon Nanotube-Based Piezoresistive Strain Sensors. *J. Sens.* **2012**, *652438*.
- Cao, J.; Wang, Q.; Dai, H. Electromechanical Properties of Metallic, Quasimetallic, and Semiconducting Carbon Nanotubes under Stretching. *Phys. Rev. Lett.* **2003**, *90*, 157601.
- Yang, L.; Han, J. Electronic Structure of Deformed Carbon Nanotubes. *Phys. Rev. Lett.* **2000**, *85*, 154.
- Kleiner, A.; Eggert, S. Band Gaps of Primary Metallic Carbon Nanotubes. *Phys. Rev. B* **2001**, *63*, 073408.
- Yang, L.; Anantram, M. P.; Han, J.; Lu, J. P. Band-Gap Change of Carbon Nanotubes: Effect of Small Uniaxial and Torsional Strain. *Phys. Rev. B* **1999**, *60* (13), 874.
- Heyd, R.; Charlier, A.; McRae, E. Uniaxial-Stress Effects on the Electronic Properties of Carbon Nanotubes. *Phys. Rev. B* **1997**, *55*, 6820.
- Nishio, T.; Miyato, Y.; Kobayashi, K.; Matsushige, K.; Yamada, H. Piezoresistive Properties of Carbon Nanotubes under Radial Force Investigated by Atomic Force Microscopy. *Appl. Phys. Lett.* **2008**, *92*, 063117.
- Maiti, A.; Sivžhenko, A.; Anantram, M. P. Electronic Transport through Carbon Nanotubes: Effects of Structural Deformation and Tube Chirality. *Phys. Rev. Lett.* **2002**, *88*, 126805.
- Gulseren, O.; Yildirim, T.; Ciraci, S.; Klč, C. Reversible Band-Gap Engineering in Carbon Nanotubes by Radial Deformation. *Phys. Rev. B* **2002**, *65*, 155410.
- Koziol, K.; Vilatela, J.; Moisala, A.; Motta, M.; Cunniff, Ph.; Sennett, M.; Windle, A. High-Performance Carbon Nanotube Fiber. *Science* **2007**, *318*, 1892.
- Motta, M.; Moisala, A.; Kinloch, I. A.; Windle, A. H. High Performance Fibres from 'Dog Bone' Carbon Nanotubes. *Adv. Mater.* **2007**, *19*, 3721.
- Cullinan, M.; Culpepper, M. Carbon Nanotubes as Piezoresistive Microelectromechanical Sensors: Theory and Experiment. *Phys. Rev. B* **2010**, *82*, 115428.
- Mallik, N.; Schulz, M. J.; Shanov, V. N.; Hurd, D.; Chakraborty, S.; Jayasinghe, Ch.; Abot, J.; Song, A. Study on Carbon Nano-Tube Spun Thread as Piezoresistive Sensor Element. *Adv. Mater. Res.* **2009**, *67*, 155.
- Zhao, H.; Zhang, Y.; Bradford, Ph. D.; Zhou, Q.; Jia, Q.; Yuan, F.-G.; Zhu, Y. Carbon Nanotube Yarn Strain Sensors. *Nanotechnology* **2010**, *21*, 305502.
- Qiu, J.; Terrones, J.; Vilatela, J. J.; Vickers, M. E.; Elliott, J. A.; Windle, A. H. Liquid Infiltration into Carbon Nanotube Fibers: Effect on Structure and Electrical Properties. *ACS Nano* **2013**, *7*, 8412–8422.
- Xu, F.; Sadrzadeh, A.; Xu, Z.; Yakobson, B. Can Carbon Nanotube Fibers Achieve the Ultimate Conductivity?—Coupled-Mode Analysis for Electron Transport Through the Carbon Nanotube Contact. *J. Appl. Phys.* **2013**, *114*, 063714.
- Yu, A. Y. Electron Tunneling and Contact Resistance of Metal-Silicon Contact Barriers. *Solid-State Electron.* **1970**, *13*, 239–247.
- Janas, D.; Koziol, K. K. Rapid Electrothermal Response of High-Temperature Carbon Nanotube Film Heaters. *Carbon* **2013**, *59*, 457–463.
- Vilatela, J. J.; Windle, A. H. A Multifunctional Yarn Made Of Carbon Nanotubes. *J. Eng. Fiber. Fabr.* **2012**, *7*, 23–28.
- Hunter, R. J. *Introduction to Modern Colloid Science*; Oxford University Press: Oxford, UK, 1993.
- Rouquerol, F.; Rouquerol, J.; Sing, K. Adsorption by Powders and Porous Solids Principles. *Methodology and Applications*; Academic Press: London, UK, 1999.
- Lekawa-Raus, A. Carbon Nanotube Fibres for Electrical Wiring Applications, Ph.D. Thesis, University of Cambridge, UK, 2013.
- [www.textechno.com](http://www.textechno.com) (accessed May 2014).